Eur. Phys. J. B **3**, 427–435 (1998)

THE EUROPEAN PHYSICAL JOURNAL B

Charge correlations in the weakly doped t−J model calculated by projection technique

M. Vojta[a] and K.W. Becker

Institut für Theoretische Physik, Technische Universität Dresden, 01062 Dresden, Germany

Received: 10 July 1997 / Revised: 19 March 1998 / Accepted: 3 April 1998

Abstract. We study frequency- and wave-vector dependent charge correlations in weakly doped antiferromagnets using Mori-Zwanzig projection technique. The system is described by the two-dimensional t-J model. The ground state is expressed within a cumulant formalism which has been successfully applied to study magnetic properties of the weakly doped system. Within this approach the ground state contains independent spin-bag quasiparticles (magnetic polarons). We present results for the charge-density response function and for the optical conductivity at zero temperature for different values of t/J. They agree well with numerical results calculated by exact diagonalization techniques. The density response function for intermediate and large momenta shows a broad continuum on energy scales of order of several t whereas the optical conductivity for $\omega > 0$ is dominated by low energy excitations (at 1.5–2J). We show that these weak-doping properties can be well understood by transitions between excited states of spin-bag quasiparticles.

PACS. 74.25.Fy Transport properties (electric and thermal conductivity thermoelectric effects, etc.) – 75.10.Jm Quantized spin models – 75.50.Ee Antiferromagnetics

1 Introduction

The discovery of the high-temperature superconductivity has increased the interest in strongly correlated electronic systems. Many properties of the superconducting cuprates are still not completely understood, an effective theory capable of modeling the ground state and the excitations of these materials remains an outstanding problem. Among the interesting features in the optical response of the cuprate materials are mid-infrared (MIR) structures at energies at 0.2-0.5 eV, see *e.g.* [1,2]. Their origin has been discussed extensively and is not yet completely clarified.

The one-band Hubbard model and the t-J model are two candidates for a description of the copper-oxide planes. The purpose of this paper is an analytical study of the dynamical charge response and the optical conductivity in the weakly doped t-J model at finite energies and zero temperature.

Theoretical progress in this field is mostly based on numerical techniques, especially on exact diagonalization methods [3–6] and Lanczos calculations [7]. However, the small system sizes presently accessible to numerical methods leave many problems unresolved. So it is often not obvious whether the structures observed in the spectra obtained from small-cluster calculations are finite-size effects or bulk properties. Finite-size scaling is hard to perform for two-dimensional systems because of the limited number of cluster sizes. Small but finite momenta and hole concentrations cannot be investigated by numerics.

The spin response of doped antiferromagnets has also been studied in a number of analytical papers but only few authors have investigated the optical conductivity and the charge density response function [8–12]. The low-energy part of the optical conductivity has been found to fall off slower than predicted by Drude theory; a pronounced MIR structure is visible especially at zero or low temperature ($T \ll t, J$) and small doping ($\delta < 10\%$). Some of the analytical results indicate sharp peaks in the density response at large momenta [8,9]. A recent slave-boson approach [11] yields one broad structure at high energy in this regime which is consistent with numerical studies. Besides the above mentioned fermionic models also boson models have been studied, *e.g.* bosons (representing holes) coupled to a fluctuating gauge field [10]. This coupling leads to an incoherent density fluctuation spectrum at finite temperatures.

The system we are interested in here is the 2D t-J model [13,14]:

$$H = -t \sum_{\langle ij \rangle \sigma} (\hat{c}^\dagger_{i\sigma} \hat{c}_{j\sigma} + \hat{c}^\dagger_{j\sigma} \hat{c}_{i\sigma}) + J \sum_{\langle ij \rangle} \left(\mathbf{S}_i \mathbf{S}_j - \frac{n_i n_j}{4} \right). \tag{1}$$

$\mathbf{S}_i$ is the local electronic spin operator and n_i the electron number operator at site i. The symbol $\langle ij \rangle$ refers to

[a] e-mail: vojta@theory.phy.tu-dresden.de

a summation over pairs of nearest neighbors. At half filling the t-J Hamiltonian reduces to the antiferromagnetic Heisenberg model. The electronic creation operators $\hat{c}^\dagger_{i\sigma}$ exclude double occupancies:

$$\hat{c}^\dagger_{i\sigma} = c^\dagger_{i\sigma}(1 - n_{i,-\sigma}). \tag{2}$$

The t-J model (1) is by now believed to describe the relevant low-energy degrees of freedom of the copper-oxide planes in the high-T_c materials. So we expect our results to coincide with experimental observations in the underdoped compounds at low energies only (1 eV and below). Excitations at higher energies of course are not covered by the t-J Hamiltonian.

We study the time- and wave-vector dependent charge-charge correlation function defined by

$$G_{\rho\rho}(\mathbf{k}, t) = \langle\psi_0|\rho^{el\dagger}_{\mathbf{k}}\rho^{el}_{\mathbf{k}}(-t)|\psi_0\rangle. \tag{3}$$

The corresponding Laplace transform can be written as

$$G_{\rho\rho}(\mathbf{k}, \omega) = \langle\psi_0|\rho^{el\dagger}_{\mathbf{k}}\frac{1}{z - L}\rho^{el}_{\mathbf{k}}|\psi_0\rangle, \quad z = \omega + i\eta,\ \eta \to 0. \tag{4}$$

Here, $\rho^{el}_{\mathbf{k}} = \sum_{\mathbf{q},\sigma} c^\dagger_{\mathbf{k}+\mathbf{q},\sigma}c_{\mathbf{q}\sigma} = \sum_{i\sigma} e^{i\mathbf{k}\mathbf{R}_i}c^\dagger_{i\sigma}c_{i\sigma}$ is the Fourier-transformed charge density operator. $|\psi_0\rangle$ denotes the exact ground state of the system, and z is the complex frequency variable. The Liouville operator L is a superoperator defined by $LA = [H, A]_-$ for any operator A. At zero temperature the optical conductivity $\sigma(\omega)$ for frequencies $\omega > 0$ is related to the charge response function $G_{\rho\rho}(\mathbf{k}, \omega)$ as follows:

$$Re\big(\sigma(\omega)\big) = \frac{e^2}{cN}\lim_{\mathbf{k}\to 0}\frac{\omega\, Im\big(G_{\rho\rho}(\mathbf{k}, \omega)\big)}{\mathbf{k}^2} \tag{5}$$

where N is the total particle number. Equation (5) follows from the continuity relation $L\rho^{el}_{\mathbf{k}} = \mathbf{k}\cdot\mathbf{j}_{\mathbf{k}}$ where $\mathbf{j}_{\mathbf{k}}$ is the Fourier-transformed charge current density operator.

Due to strong correlations usual diagrammatic techniques based on Wick's theorem can not be easily applied to solve the Hamiltonian (1). Neither the first nor the second part is bilinear in fermion operators, and the creation and annihilation operators $\hat{c}^\dagger_{i\sigma}$ and $\hat{c}_{i\sigma}$ do not obey simple anticommutation relations. For this reason, non-standard analytical methods like variational wavefunctions, coupled-cluster methods, slave-boson and slave-fermion techniques or 1/N expansions have been applied to the 2D t-J model and related strongly correlated systems.

In the following, a projection technique [15–17] approach based on the introduction of cumulants to evaluate charge density response functions is presented. We focus here on the finite-energy contributions: since we do not consider the diamagnetic part of the current we do not obtain results for the response at zero energy, so the present calculation does not yield a Drude-like contribution to $\sigma(\omega)$. In a recent letter [18] we have published first results for $G_{\rho\rho}(\mathbf{k}, \omega)$ and $\sigma(\omega)$ using the present method. Here we employ an improved set of projection variables and present more details of the calculation. At intermediate and large momenta we find for the density response function a broad continuum of excitations on energy scales of several t. The optical conductivity for finite ω is dominated by a small number of peaks at low energies of order J. The features and the different scaling behavior of these spectra can be explained in terms of internal degrees of freedom of the spin-bag quasiparticles.

The paper is organized as follows: in Section 2 we briefly sketch the cumulant method proposed in references [19–21] and show how to calculate dynamical correlation functions. The description of the ground state of the weakly doped t-J model within the cumulant formalism is subject of Section 3. The employed ground state wavefunction consists of independent hole quasiparticles (magnetic polarons) moving on an antiferromagnetic background. The choice of appropriate dynamical variables for the projection technique is shown in Section 4. The variables are constructed from path operators which form the hole quasiparticles. In Section 5 we present results for the charge-charge correlation function and the optical conductivity. They will be compared with results from numerical investigations found in the literature. A discussion of the results will close the paper.

2 Cumulant method for correlation functions

A recently introduced approach for calculating expectation values and dynamical correlation functions [19–21] is based on the introduction of cumulants. Provided that the Hamiltonian of the system can be split into an unperturbed part H_0 and a perturbation H_1, $H = H_0 + H_1$, with eigenstates and eigenvalues of H_0 known, this method uses the decomposition

$$e^{-\lambda H} = e^{-\lambda(H_1 + L_0)}\, e^{-\lambda H_0}. \tag{6}$$

This relation can be proved by comparing the equations of motion of either side with respect to λ. L_0 is the Liouville operator corresponding to H_0, defined by the relation $L_0 A = [H_0, A]_-$ for any operator A. Let us denote the ground state of the unperturbed Hamiltonian H_0 by $|\phi_0\rangle$ and its energy by ϵ_0

$$H_0|\phi_0\rangle = \epsilon_0|\phi_0\rangle. \tag{7}$$

Here we are interested in calculating dynamical correlation functions of operators B_ν

$$G_{\nu\mu}(\omega) = \langle\psi_0|\delta B^+_\nu\frac{1}{z - L}\delta B_\mu\,|\psi_0\rangle \tag{8}$$

where we have introduced $\delta B_\nu = B_\nu - \langle\psi_0|B_\nu|\psi_0\rangle$. Using (6) one can show [21] that these correlation functions can be rewritten as

$$G_{\nu\mu}(\omega) = \langle\phi_0|\Omega^+ B^+_\nu\left(\frac{1}{z - L}B_\mu\right)^{\cdot}\Omega|\phi_0\rangle^c. \tag{9}$$

The operator Ω has similarity to the so-called wave operator (or Moeller operator known from scattering theory). Within cumulants it transforms the ground state $|\phi_0\rangle$ of the unperturbed system into the exact ground state $|\psi_0\rangle$ of H. Explicitly it is given by

$$\Omega = 1 + \lim_{x\to 0} \frac{1}{x - (L_0 + H_1)} H_1. \tag{10}$$

The brackets $\langle\phi_0|\,...\,|\phi_0\rangle^c$ denote cumulant expectation values formed with $|\phi_0\rangle$. The dot $\cdot$ indicates that the quantity inside $(...)^{\cdot}$ has to be treated as a single entity in the cumulant formation. For a detailed discussion of cumulants see *e.g.* Kubo [22].

The relation (9) can be applied to either weakly or strongly correlated systems because its use is independent of the operator statistics, *i.e.*, it is valid for fermions, bosons or spins. Note that cumulants ensure size consistency for any subsequent approximations for the wave operator Ω.

Using Mori-Zwanzig projection technique [15,16] one can derive the following set of equations of motion for the dynamical correlation functions $G_{\nu\mu}(\omega)$:

$$\sum_\nu \left(z\delta_{\eta\nu} - \omega_{\eta\nu} - \Sigma_{\eta\nu}(\omega)\right) G_{\nu\mu}(\omega) = \chi_{\eta\mu}. \tag{11}$$

$\chi_{\eta\nu}$, $\omega_{\eta\nu}$, and $\Sigma_{\eta\nu}$ are the static correlation functions, frequency terms, and self-energies, respectively. They are given by the following cumulant expressions:

$$\begin{aligned}
\chi_{\eta\nu} &= \langle\phi_0|\Omega^+ B_\eta^+ B_\nu\, \Omega|\phi_0\rangle^c, \\
\omega_{\eta\nu} &= \sum_\lambda \langle\phi_0|\Omega^+ B_\eta^+ (LB_\lambda)^{\cdot}\, \Omega|\phi_0\rangle^c \chi^{-1}_{\lambda\nu}, \\
\Sigma_{\eta\nu}(\omega) &= \sum_\lambda \langle\phi_0|\Omega^+ B_\eta^+ \left(LQ\frac{1}{z - QLQ}QLB_\lambda\right)^{\cdot} \\
&\quad \times \Omega|\phi_0\rangle^c \chi^{-1}_{\lambda\nu},
\end{aligned} \tag{12}$$

$\chi^{-1}_{\nu\mu}$ is the inverse matrix of $\chi_{\nu\mu}$, and Q is given by

$$Q = 1 - P, \quad P = \sum_{\nu\mu} B_\nu\, \Omega|\phi_0\rangle^c \chi^{-1}_{\nu\mu} \langle\phi_0|\Omega^+ B_\mu^+\,. \tag{13}$$

P denotes a projection operator projecting onto the subspace of the Liouville space spanned by the operators B_ν, Q projects onto the complementary subspace.

The described cumulant version of projection technique has a conceptual advantage compared to standard projection technique. Using projection technique the Laplace transform of a correlation function may be written as a continued fraction expansion (or a set of equations of motion) describing the dynamics of the system. The continued fraction contains expectation values which are static quantities. These expectation values have to be evaluated with the ground state of the interacting system. In standard projection technique this has to be done separately using mean-field methods or perturbation theory. In contrast, in the cumulant approach static and dynamical aspects of the system are treated along the same lines. For a further discussion see [21].

3 Ground state wavefunction

Now we turn to the t-J model at weak doping. The description of the ground state within the cumulant formalism used here has been shown to produce reasonable results for the doping dependence of the staggered magnetization and the spin-wave spectrum of the antiferromagnetic phase of the doped system [23].

In the following δ denotes the hole concentration away from half filling. Our system with N lattice sites possesses $M = \delta N$ dopant holes. The Hamiltonian is decomposed into H_0 and H_1 as follows:

$$H_0 = H_{Ising} = J\sum_{\langle ij\rangle}(S_i^z S_j^z - \frac{n_i n_j}{4}) + J(N - 2M), \tag{14}$$

$$\begin{aligned}
H_1 &= H_t + H_\perp \\
&= -t \sum_{\langle ij\rangle,\sigma} (\hat{c}^+_{i\sigma}\hat{c}_{j\sigma} + \hat{c}^+_{j\sigma}\hat{c}_{i\sigma}) + \frac{J}{2}\sum_{\langle ij\rangle}(S_i^- S_j^+ + S_i^+ S_j^-).
\end{aligned}$$

The ground state $|\phi_0\rangle$ of the unperturbed Hamiltonian H_0 is an antiferromagnetically ordered Néel state with M holes. The holes have fixed momenta $\mathbf{k}_m$ and are located on the sublattice σ_m ($\sigma_m = \uparrow, \downarrow$)

$$\begin{aligned}
|\phi_0\rangle &= \hat{c}_{\mathbf{k}_1\sigma_1}\,\ldots\,\hat{c}_{\mathbf{k}_M\sigma_M}|\phi_{N\acute{e}el}\rangle \\
&= \frac{1}{(N/2)^{M/2}} \prod_{m=1}^{M} \left(\sum_{i_m\in\sigma_m} e^{\mathrm{i}\,\mathbf{k}_m\mathbf{R}_{i_m}}\,\hat{c}_{i_m\sigma_m}\right)|\phi_{N\acute{e}el}\rangle.
\end{aligned} \tag{15}$$

In H_0 we have shifted the energy level so that $\langle\phi_0|H_0|\phi_0\rangle = 0$.

Within the cumulant method we employ an exponential ansatz [24] for the wave operator Ω, $\Omega = e^S$. Here, the operator S contains the effect of the perturbation H_1 onto the unperturbed ground state $|\phi_0\rangle$. We have to consider two parts of H_1, the spin-flip term $H_\perp$ and the hopping term H_t.

The hole motion processes induced by H_t are described by path operators [25–28] which leads to the picture of spin-bag quasiparticles [29]. Here we define path concatenation operators $A_{n,\xi}(i)$ where i denotes a lattice site, n the path length, and ξ the individual path shape: $A_{n,\xi}(i)$ operating on the Néel state with one hole at site i, $\hat{c}_{i\uparrow}|\phi_{N\acute{e}el}\rangle$, moves the hole n steps away and creates a path or string ξ of n spin defects attached to the transferred hole. For $n = 1$ there are 4 different path shapes (Fig. 1), for $n = 2$ there are 12 and so on. Explicitly, the operators $A_{n,\xi}(i)$ for sites i on the $\uparrow$-sublattice are defined by

$$\begin{aligned}
A_{1,\xi}(i) &= \sum_j \hat{c}_{j\downarrow}\hat{c}^+_{i\downarrow} R^\xi_{ji}, \\
A_{2,\xi}(i) &= \sum_{jl} \hat{c}_{l\uparrow} S_j^+ \hat{c}^+_{i\downarrow} R^\xi_{lji}, \quad (i\in\uparrow,\, j\in\downarrow,\, l\in\uparrow,\, m\in\downarrow) \\
A_{3,\xi}(i) &= \sum_{jlm} \hat{c}_{m\downarrow} S_l^- S_j^+ \hat{c}^+_{i\downarrow} R^\xi_{mlji}, \quad \ldots
\end{aligned} \tag{16}$$

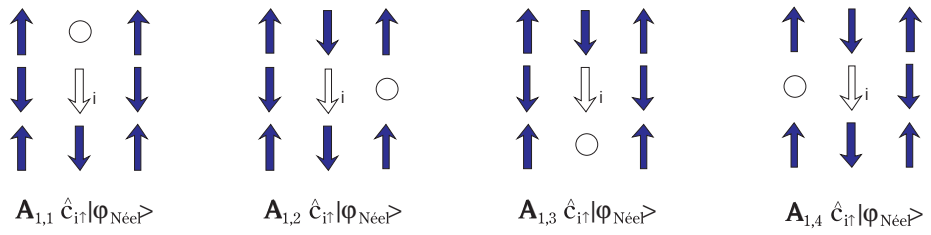

Fig. 1. Path shapes of length 1 created by the operators $A_{1,\xi}$ acting on a hole at site i in the $\uparrow$-sublattice.

The operators $A_{n,\xi}$ for sites i on the "down" sublattice are defined analogously with all spins reversed. The matrices $R^{\xi}_{i_n \ldots i_1}$ allow the hole to jump along a path of shape ξ:

$$R^{\xi}_{i_n \ldots i_1} = \begin{cases} 1 & i_1, ..., i_n \text{ connected by path of shape } \xi \\ 0 & \text{otherwise.} \end{cases} \tag{17}$$

Having defined the excitation operators $A_{n,\xi}(i)$ the wave operator Ω used for the cumulant formalism takes the form

$$\Omega = \exp\left(\sum_{n=1}^{n_{max}} \sum_{\xi=1}^{m_n} \lambda_{n,\xi} A_{n,\xi}\right), \; A_{n,\xi} = \sum_i A_{n,\xi}(i) \tag{18}$$

with parameters $\lambda_{n,\xi}$ yet unknown. Note the additional definiton $A_0(i) = \frac{1}{2}\sum_\sigma \hat{c}_{i\sigma}\hat{c}^\dagger_{i\sigma} = (1 - n_{i\uparrow})(1 - n_{i\downarrow})$ which is the only "path" with zero length ($\xi = 1$). This operator is a projection operator on the empty state at site i. The path operators $A_{n,\xi}$ commute with each other because they only contain spin-flip operators destroying Néel order. Applying the operator Ω (18) to the unperturbed ground state (15) adds to each hole a cloud of spin defects leading to a spin bag or magnetic polaron [28,29]. In the ansatz (18) we use separate coefficients $\lambda_{n,\xi}$ for all individual paths $A_{n,\xi}$. This is an extension compared to the ansatz of reference [23] where all paths with the same length n had been given the same weight. The additional degrees of freedom improve the ground-state wavefunction for non-zero hole momentum taking into account that the quasiparticle state is not exactly s-like, see also Section 5.3.

The transverse part $H_\perp$ of the magnetic exchange creates or destroys pairs of spin defects and therefore can change the length of a given path of spin defects by 2. This process leads to a coherent motion of the hole quasiparticle through the lattice [26,27].

Additional spin fluctuations in the antiferromagnetic background will be neglected here. The results show that this approximation gives already reliable results for the charge density response of the system because the charge dynamics is mainly determined by the motion of the hole quasiparticles. However, for a description of magnetic properties or the spin response of the system these ground-state spin fluctuations would be essential, see *e.g.* [23].

The coefficients $\lambda_{n,\xi}$ of the ansatz (18) are determined by the condition for $\Omega|\phi_0\rangle$ to be an eigenstate of H. Following reference [24] one arrives at a non-linear set of equations for the ground-state energy E_0 and the coefficients $\lambda_{n,\xi}$:

$$\begin{aligned} E_0 &= \langle\phi_0|H\Omega|\phi_0\rangle^c, \\ 0 &= \langle\phi_0|A^\dagger_{n,\xi} H\Omega|\phi_0\rangle^c \end{aligned} \tag{19}$$

with Ω given by (18). The cumulant expectation values have to be taken with respect to the unperturbed ground state (15). The set of equations (19) together with the additional approximation of independent hole quasiparticles leads to a generalized eigenvalue problem. For details see reference [23]. The total ground-state energy depends on the initial momenta of the hole quasiparticles $\mathbf{k}_m$ in (15). The energy minimum for the one-hole problem is located at $\mathbf{k} = (\pm\pi/2, \pm\pi/2)$ which leads to a hole-pocket Fermi surface. Further properties of the one-hole spectrum are discussed in Section 5.3. The used picture of independent quasiparticles is appropriate for small hole concentrations, *i.e.*, for a dilute gas of holes moving in an antiferromagnetic background.

4 Dynamical variables for charge correlations

To calculate dynamical charge correlation functions we employ the cumulant version of Mori-Zwanzig projection technique as described in Section 2. At first we have to choose a set of relevant operators B_ν. Here we are going to neglect the self-energy terms $\Sigma_{\nu\mu}$ from (12). This can be done using a sufficiently large set of operators B_ν to cover the charge dynamics we are interested in.

One variable to be included is the charge density operator itself. Note that the particle density $\rho^{el}_{\mathbf{k}} = \sum_{i\sigma} e^{i\mathbf{k}\mathbf{R}_i}\hat{c}^\dagger_{i\sigma}\hat{c}_{i\sigma}$ and the hole density $\rho^{hole}_{\mathbf{k}} = \frac{1}{2}\sum_{i\sigma} e^{i\mathbf{k}\mathbf{R}_i}\hat{c}_{i\sigma}\hat{c}^\dagger_{i\sigma} = \sum_{i\sigma} e^{i\mathbf{k}\mathbf{R}_i} A_0(i)$ are equivalent quantities according to

$$\rho^{hole}_{\mathbf{k}} + \rho^{el}_{\mathbf{k}} = \sum_{i\sigma} e^{i\mathbf{k}\mathbf{R}_i}\left(\frac{1}{2}\hat{c}_{i\sigma}\hat{c}^\dagger_{i\sigma} + \hat{c}^\dagger_{i\sigma}\hat{c}_{i\sigma}\right) = N\,\delta_{\mathbf{k},0}. \tag{20}$$

Note that $\sum_\sigma(\frac{1}{2}\hat{c}_{i\sigma}\hat{c}^\dagger_{i\sigma} + \hat{c}^\dagger_{i\sigma}\hat{c}_{i\sigma})$ is the projector on the empty and singly occupied states at site i.

As first variable we therefore choose $\rho^{hole}_{\mathbf{k}}$. Additional dynamical variables B_ν can be deduced from the action the Liouville operator to the first variable $\rho^{hole}_{\mathbf{k}}$, *i.e.* from

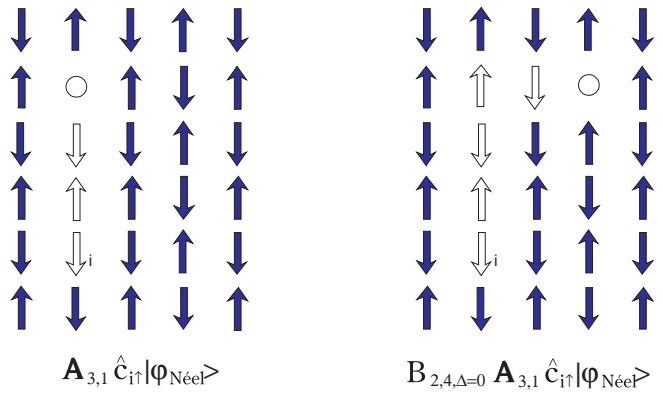

Fig. 2. Effect of $B_{2,4,0}$ on a path of length 3 created by $A_{3,1}$.

$L\,\rho_{\mathbf{k}}^{hole}$, $L(L\,\rho_{\mathbf{k}}^{hole})$ *etc.* All variables should provide particle number conservation because H and the density operator do not change the total number of particles.

The hopping part of L creates strings of spin defects when applied to $\rho_{\mathbf{k}}^{hole}$, *i.e.*, $L_t^n\,\rho_{\mathbf{k}}^{hole}$ is a sum of path concatenation operators up to length n. The spin-flip part $L_\perp$ creates or destroy pairs of spin defects. It neglected or changed the length of a spin-defect path by 2. Additional processes connecting paths of different holes, *i.e.* hole-hole interactions, will be neglected consistently with the ground state evaluation procedure. Assuming that the charge dynamics is mainly carried by the spin-bag quasiparticles we define a set of variables which contains the processes described above:

$$\begin{aligned} B_{n,\xi,\boldsymbol{\Delta}}(\mathbf{k}) &= \sum_{i,\sigma} e^{\mathrm{i}\mathbf{k}\mathbf{R}_i} (A_{n,\xi}(i+\boldsymbol{\Delta})\hat{c}_{i+\boldsymbol{\Delta},\sigma})(A_0(i)\hat{c}_{i\sigma})^\dagger \\ &= \sum_{i,\sigma} e^{\mathrm{i}\mathbf{k}\mathbf{R}_i}\, B_{n,\xi,\boldsymbol{\Delta}}(i) \end{aligned} \tag{21}$$

where $A_{n,\xi}(i)$ is a path operator of length n with the path shape ξ acting on a hole at site i, as defined in the previous section. The indices $n, \xi, \boldsymbol{\Delta}$ replace the general index ν of the dynamical variables B_ν in equations (8, 9). The operator $B_{n,\xi,\boldsymbol{\Delta}}$ couples to a hole at site i destroying it, creates a hole at site $\mathbf{R}_i + \mathbf{R}_{\boldsymbol{\Delta}}$ and adds the path $A_{n,\xi}$. Here, $\mathbf{R}_{\boldsymbol{\Delta}}$ is a vector connecting two sites on the same sublattice, $i+\boldsymbol{\Delta}$ is a short-hand notation for $\mathbf{R}_i+\mathbf{R}_{\boldsymbol{\Delta}}$. As an example, Figure 2 shows the effect of the variable $B_{2,4,0}$ applied to a path state $A_{3,1}\hat{c}_{i\uparrow}|\phi_{N\acute{e}el}\rangle$. Variables with $\boldsymbol{\Delta} \neq 0$ arise from the application of $H_\perp$ at sites at the beginning of a spin-defect path. Such a process shortens the path by 2 and moves the initial site of the quasiparticle (the path starting point) two sites away ($|\mathbf{R}_{\boldsymbol{\Delta}}| = 2$). The operators $B_{n,\xi,\boldsymbol{\Delta}}$ provide a coupling between the ground state and excited states of the spin-bag quasiparticles, see Section 5.3. So the relevant part of the Liouville space spanned by the operators $B_{n,\xi,\boldsymbol{\Delta}}$ contains all individual path states of the holes. Note that the first of these operators is the hole density operator itself:

$$B_{0,1,0}(\mathbf{k}) = \rho_{\mathbf{k}}^{hole} = \frac{1}{2}\sum_{i\sigma} e^{\mathrm{i}\mathbf{k}\mathbf{R}_i}\,\hat{c}_{i\sigma}\hat{c}_{i\sigma}^\dagger. \tag{22}$$

The quantity we are interested in is therefore the diagonal correlation function $G_{\nu\nu}(\mathbf{k}, z)$ with $\nu = (0, 1, 0)$.

Additional projection variables could be found by applying the spin-flip term $H_\perp$ to $B_{n,\xi,\boldsymbol{\Delta}}$ at sites along the path. Those variables would provide a coupling to states with spin fluctuations separated from the spin-bag quasiparticles. Such processes would describe scattering of the quasiparticle states with spin waves, they will be neglected here.

The above set of dynamical variables is an extension of the one used in previous calculations [18]. There we had included only variables with $\boldsymbol{\Delta} = 0$. The new variables with $\boldsymbol{\Delta} \neq 0$ provide additional degrees of freedom being useful if more than one hole is present in the system. This can be easily understood from a comparison with the density response of a system of free fermions: the correct excitations are obtained there if one splits the density $\rho_{\mathbf{k}} = \sum_{\mathbf{q}} c_{\mathbf{k}+\mathbf{q}}^\dagger c_{\mathbf{q}} = \sum_i e^{\mathrm{i}\mathbf{k}\mathbf{R}_i} c_i^\dagger c_i$ into a set of dynamical variables $\{c_{\mathbf{k}+\mathbf{q}}^\dagger c_{\mathbf{q}}\}$ where $\mathbf{q}$ are the momenta of the particles present in the ground state. An equivalent set of variables can be obtained from linear combinations of the $\{c_{\mathbf{k}+\mathbf{q}}^\dagger c_{\mathbf{q}}\}$ leading to $\{\sum_i e^{\mathrm{i}\mathbf{k}\mathbf{R}_i} c_{i+\boldsymbol{\Delta}}^\dagger c_i\}$ which correspond to the $B_{n,\xi,\boldsymbol{\Delta}}$ of the present calculation.

Having chosen the set of projection variables (21) we can consider the equations of motion (11) for the correlation functions of the operators $B_{n,\xi,\boldsymbol{\Delta}}$. The relevant terms for the dynamics are the static correlation functions and the frequency terms given in (12). The arising cumulant expectation values can be transformed to normal expectation values according to Appendix A. Calculating the matrix elements we have neglected hole-hole interaction processes and geometry effects such as spiral paths. Within these approximations the path operators form an orthogonal basis set,

$$\langle\phi_0|A_{n,\xi}^\dagger A_{m,\eta}|\phi_0\rangle = M\,\delta_{nm}\delta_{\xi\eta}, \tag{23}$$

where M is the number of holes present in the system. The static matrix χ from (12) therefore becomes proportional to a unity matrix:

$$\langle\phi_0|\Omega^\dagger\, B_{n,\xi,\boldsymbol{\Delta}}^\dagger\, B_{m,\eta,\boldsymbol{\Theta}}\,\Omega|\phi_0\rangle^c = M\,\delta_{nm}\delta_{\xi\eta}\delta_{\boldsymbol{\Delta}\boldsymbol{\Theta}}. \tag{24}$$

The elements of the frequency matrix from (12) contain the hole motion processes. To be short, here we only state the results for one hopping process:

$$\begin{aligned} &\langle\phi_0|\Omega^\dagger\, B_{n,\xi,\boldsymbol{\Delta}}^\dagger (L_t\, B_{m,\eta,\boldsymbol{\Theta}})^\cdot\,\Omega|\phi_0\rangle^c \\ &\qquad = t\,M(\delta_{n\xi,m\eta+1} + \delta_{n\xi+1,m\eta})\delta_{\boldsymbol{\Delta}\boldsymbol{\Theta}} \end{aligned} \tag{25}$$

where $\delta_{n\xi,m\eta+1}$ is 1 if the path $A_{n\xi}$ is obtained from $A_{m\eta}$ by one further hopping process, otherwise it is zero. For more details concerning the matrix elements we refer to a recent publication [30].

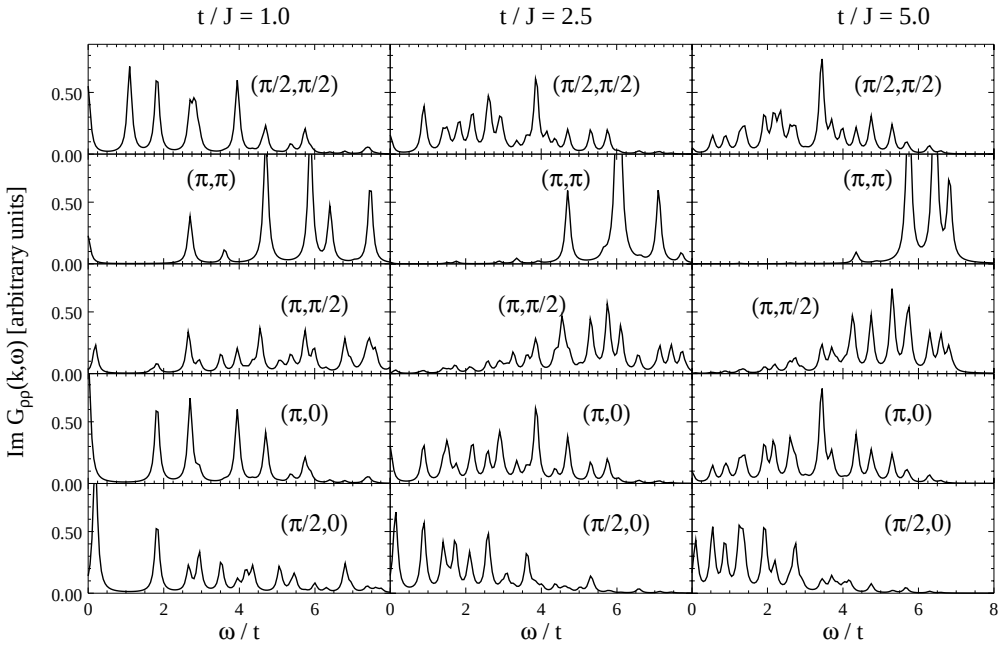

Fig. 3. Charge response functions obtained from the present calculation for very small δ, different momentum transfers and parameter values t/J=1, 2.5, and 5. The peaks are plotted with Lorentzians using an artificial linewidth of $0.1t$.

5 Results

In the numerical calculations we have included paths up to length 5 which gives a set of 485 path variables $A_{n,\xi}$. The system has a few holes ($\delta \ll 1$) in each of the four hole pockets (at momenta $(\pm\pi/2, \pm\pi/2)$). It can be shown that in this case four different vectors $\boldsymbol{\Delta}$ in the set of dynamical variables are sufficient to describe the charge dynamics at low doping. Note that this approximation does not take into account changes of the hole Fermi surface with doping, so our treatment is strictly valid only in the limit of $\delta \to 0$. These Fermi surface changes would be important for a good description of the low-energy intraband excitations of the hole quasiparticles at non-zero doping (see below).

We have tested maximum path lengths of 2, 3, 4, and 5. Beyond a path length of 2 we obtained no essential differences in the spectra except of richer structures with an increasing number of projection variables. Thus we expect only minor changes when including longer paths, see Section 5.3.

5.1 Charge correlation function

Results for the charge response function $G_{\rho\rho}(\mathbf{k}, \omega)$ at t/J = 1, 2.5, and 5 are shown in Figure 3. Note that we obtain discrete spectra because we have neglected all self-energies. In the figures we have introduced Lorentzians with a small artificial linewidth. The main doping dependence of the spectra is found in the intensity which is proportional to the hole concentration. This follows from the assumption of independent hole motion and a doping-independent spin background (rigid-band picture). Within these approximations all matrix-elements in (12) are essentially proportional to the hole concentration δ. From (11) it is seen that therefore all correlation functions $G_{\nu\mu}$ are proportional to δ.

For smaller momentum the spectral weight is mainly concentrated in a peak near $\omega = 0$. With increasing momentum we find a transfer of spectral weight to higher energies. The figures for different values of t/J show that the broad structures observed in the spectra for large momenta scale with t, *e.g.*, the maximum spectral weight in the charge-response function at (π, π) remains at energies of about $6t$ independent of t/J. This scaling behavior will be discussed in the following sections.

Next we compare our data with Exact Diagonalization (ED) results. Due to the small cluster sizes no numerical spectra are available for small hole concentrations. Figure 4. shows a comparison of our data for $t/J = 2.5$ with ED data for $\delta = 25\%$ taken from reference [3]. It is remarkable that even for this large hole concentration we observe a qualitatively good agreement with our spectra: both results show the weight transfer to higher energies with increasing momentum and a broad continuum of excitations at large momenta. Differences may be either due to the small number of sites in the numerical calculations (which leads to an energy gap in all spectra and other finite-size effects) or due to the neglection of relaxation processes (which would produce finite linewidths) and Fermi-surface effects (which would affect the low-energy spectrum for non-zero doping) in the present calculation.

5.2 Optical conductivity

Using equation (5) one can deduce the optical conductivity from the calculated charge response function. Results for $Re(\sigma(\omega))$ are displayed in Figure 5. We find a few peaks at low energy, the positions of these main peaks scale with J. These features at $1.5-2J$ were also found in

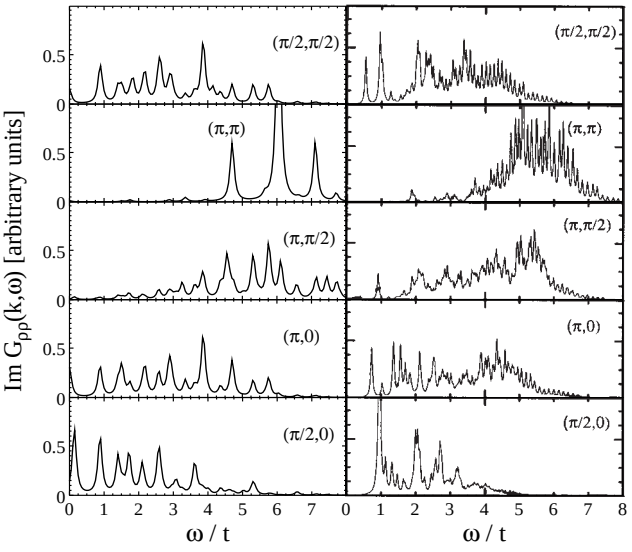

Fig. 4. Left panel: charge response function from Figure 3 for $t/J = 2.5$. Right panel: exact diagonalization data from [3] for comparison. $t/J = 2.5$. The numerical data have been calculated for a 4×4 periodic cluster and a hole concentration of $\delta = 25\%$.

numerical studies of the t-J and Hubbard models. They are supposed to coincide with the MIR structures observed in optical spectra of high-T_c superconductors being located at 0.2–0.5 eV (for $t \approx 0.5$ eV, $J \approx 0.15$–0.2 eV), see *e.g.* [2].

Within the present calculation we do not obtain a Drude-like contribution to $\sigma(\omega)$ since equation (5) is valid for non-zero frequency only, *i.e.*, it does not include the diamagnetic part of the current (due to the neglection of the self-energies which excludes scattering processes of the quasiparticle states and the assumption of independent hole motion the Drude contribution would have the form $D\,\delta(\omega)$). So the present calculation cannot account for analytical features as, *e.g.*, the drop-off of the Drude peak of finite ω.

Comparing our results with numerical data (at higher doping) we again observe reasonable agreement *e.g.* with the ED results from reference [6] for $\delta = 12.5\%$.

5.3 Relation to the one-particle spectrum

For the interpretation of the calculated spectra one can consider the one-hole spectrum of the Hamiltonian within our approximation. From the diagonalization of the one-hole problem in the subspace of path operators $A_{n,\xi}$ one obtains several bands for the spin-bag quasiparticles. As is well known, the lowest band has a minimum at $(\pm\pi/2, \pm\pi/2)$ and a bandwidth of about $2J$. It corresponds to a quasiparticle with s-like symmetry. The spin-bag states in the higher bands have nodes in the coefficients $\lambda_{n,\xi}$ (compare (18)). Note, however, that a classification according

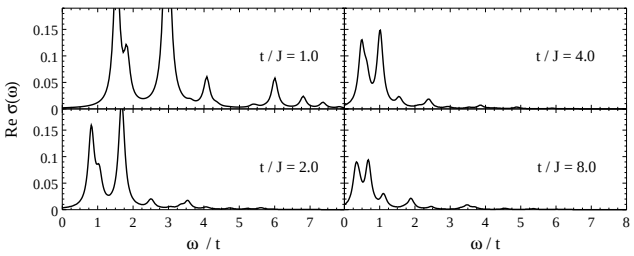

Fig. 5. Optical conductivity for small hole concentration and different t/J. The spectra have been calculated from the charge-charge correlation function using (5).

to angular momentum (p, d, f and so on) is not appropriate at least for longer paths because the path states $A_{n,\xi}$ do not obey simple rotational symmetry. The total number of one-particle states is of course equal to the number of considered path variables. Increasing the maximum path length n_{max} adds essentially many non-s-like states to the spectrum which have energies between the s-like states. So our results do not depend strongly on the maximum path length beyond $n_{max} > 2$.

The low-energy peak at small, but finite momenta is caused by excitations within the lowest quasiparticle band. These excitations are treated correctly here only for the limit $\delta \to 0$ since we have neglected changes of the Fermi surface with doping. The next structures at low energies arise from transitions between the first and second/third quasiparticle band, *i.e.*, from the s-like ground-state to p-like states. These structures are especially visible at small momentum transfer, *i.e.*, in the optical conductivity, see the discussion below. The high-energy part of the spectra corresponds to excitations to higher bands. So our calculation supports the discussion given in reference [6] where only the two low-lying states have been considered in a simplified analytical calculation for the main peak found in the optical spectrum. We want to emphasize that taking into account all string states (up to a truncation length) as done in the present work reproduces not only this main peak but the incoherent continuum at energies up to $8t$ also found in numerical work. So we have mapped the charge excitations for the t-J model (1) at small hole concentration to transitions between bands of non-interacting spin-bag quasiparticles (not taken into account are changes of the Fermi surface of these quasiparticles with doping and scattering of the quasiparticle states).

The different scaling behavior of $G_{\rho\rho}(\mathbf{k}, \omega)$ (for large $\mathbf{k}$) and $\sigma(\omega)$ with t/J arises from the internal structure of the spin-bag quasiparticles. The width of the lowest band as well as low excitation energies scale primarily with J, *i.e.*, the excitation energies can be written as $at + bJ$ with $b/a \gg t/J \approx 2 \ldots 5$. Therefore the excitation from the ground state to the first excited state has an energy of order J as seen in the optical conductivity. At large $\mathbf{k}$ the energies of the structures in the density response scale

with t. This can be understood from the following qualitative arguments: at large $\mathbf{k}$ the operator $\rho^{hole}_{\mathbf{k}}$ couples the ground state to higher excited states of the quasiparticle. This coupling depends on t/J since the quasiparticle size changes with t/J (mapping the localized hole problem onto its continuum version [31] one finds that the path coefficients decrease exponentially with a length scale proportional to $(t/J)^{1/3}$). Thus the spatial distance of the real-space nodes in the coefficients $\lambda_{n,\xi}$ increases with t/J (for fixed n, ξ), in other words, for a fixed spatial node distance the excitation number n increases with t/J. Therefore with increasing t/J the operator $\rho^{hole}_{\mathbf{k}}$ (for fixed $\mathbf{k}$) couples to higher quasiparticle states. This results in structures scaling with t in the density response function for large $\mathbf{k}$.

It is worth noting that the non-s-like states of the quasiparticle play an important role for the charge dynamics considered here. Neglecting them, *i.e.* considering all paths with the same length as ONE dynamical variable, would be a bad approximation. However, for the one-particle dynamics these states do nearly not contribute to the spectrum: if one calculates the one-hole spectral function in the subspace of path operators then only the s-like states carry considerable spectral weight. The reason for this behavior lies in the symmetry of the Hamiltonian.

6 Conclusion

In the present paper we have studied the charge dynamics in weakly doped antiferromagnets described by the t-J model at zero temperature. Our ansatz for the ground-state wave-function [23] includes mobile hole quasiparticles. Background spin fluctuations have been neglected. Thus the ground state has antiferromagnetic long-range order independent of hole doping. We have used this ground state together with a cumulant version of Mori-Zwanzig projection technique to calculate dynamical charge correlation functions.

We find structures at lower energies scaling with J for zero and small momentum and a transfer of spectral weight to higher energies with increasing momentum. At intermediate and large momenta the density response spectrum consists of a broad continuum at energies of order t. The calculations do not cover a Fermi-surface related low-energy response (including a Drude-like peak in the optical conductivity). Our results for the density response function as well as the optical conductivity are in reasonable agreement with recent numerical data obtained by exact diagonalizations [3,6,11] (see Figs. 3–5). However, these numerical calculations have been done for large hole concentrations (*e.g.*, 25%) where only short-range magnetic order is present. In contrast, our calculations are based on magnetic long-range order and neglect background spin fluctuations. Thus we conclude that the fact whether the quasiparticles move in a long-range ordered background or not does not have an essential influence on the charge response of the system at higher energies. The dynamics is determined by the local antiferromagnetic order in the vicinity of the hole quasiparticles, *i.e.*, the magnetic correlation length has to be of the order of the quasiparticle size. More precisely, our treatment is valid with antiferromagnetic order on length scales of the longest path variables included in the calculation (here 5 lattice constants). Note here that the magnetic correlation length in the high-T_c materials is about 5 lattice constants for $\delta = 12.5\%$ and about 2.5 lattice constants for $\delta = 25\%$ differing somewhat for different compounds. (Numerical simulations for the t-J and related models yield similar values although precise data cannot be obtained because of the restricted system sizes.)

A remaining task would be to include doping dependent background spin fluctuations in our ansatz for the wave operator Ω as done in the static calculations of reference [23]. The scattering of quasiparticles at spin fluctuations would cause a decay of the excited quasiparticle states and provide lifetime broadening of the lines in the response functions. From this we do not expect drastic changes in the response functions for larger energies. A second possible improvement concerns the inclusion of Fermi-surface related response at low energies, work along this line is in progress.

Appendix A: Evaluation of cumulants

In this appendix we show how to evaluate cumulants with an exponential ansatz for the wave operator Ω. The basic relation is

$$\langle\phi|\, e^{S^+} \prod_i A_i^{n_i} e^S |\phi\rangle^c = \langle\psi| \prod_i A_i^{n_i} |\psi\rangle^c \tag{A.1}$$

with A_i being arbitrary operators. Note that on the l.h.s. the operators S^+, S and A_i are subject to cumulant ordering whereas on the r.h.s. only the A_i operators are cumulant entities. However, the cumulants on the r.h.s. are formed with the new wavefunction $|\psi\rangle = e^S|\phi\rangle$.

Equation (A.1) can be proven either by integrating infinitesimal transformations $(1 + S/N)$ and using properties of cumulants [32] or by explicitly using the definition of cumulant expectation values. Here we demonstrate the second way. We start from the definition of cumulant expectation values [22] for a product of arbitrary operators A_i and an arbitrary state $|\phi\rangle$:

$$\langle\phi| \prod_i A_i^{n_i} |\phi\rangle^c = \left(\prod_i \left(\frac{\partial}{\partial \lambda_i} \right)^{n_i} \right) \ln \langle\phi| \prod_i e^{\lambda_i A_i} |\phi\rangle|_{\lambda_i = 0 \forall\, i}. \tag{A.2}$$

We consider the following expression:

$$\begin{aligned}
&\langle\phi|e^{\alpha S^+}\prod_i A_i^{n_i}\, e^{\beta S}|\phi\rangle^c \\
&= \sum_{n=0}^{\infty}\sum_{m=0}^{\infty}\frac{\alpha^n}{n!}\frac{\beta^m}{m!}\langle\phi|{S^+}^n\prod_i A_i^{n_i} S^m|\phi\rangle^c \\
&= \sum_{n=0}^{\infty}\sum_{m=0}^{\infty}\frac{\alpha^n}{n!}\frac{\beta^m}{m!}\left(\frac{\partial}{\partial\xi}\right)^n\left(\frac{\partial}{\partial\eta}\right)^m \\
&\times\left[\left(\prod_i\left(\frac{\partial}{\partial\lambda_i}\right)^{n_i}\right)\ln\langle\phi|e^{\xi S^+}\prod_i e^{\lambda_i A_i}e^{\eta S}|\phi\rangle\right]_{\substack{\xi=\eta=0\\ \lambda_i=0\forall\, i}}.
\end{aligned} \tag{A.3}$$

The last expression can be interpreted as a series expansion of the term in brackets [...] with respect to ξ and η around 0:

$$\begin{aligned}
\langle\phi|e^{\alpha S^+}\prod_i A_i^{n_i} e^{\beta S}|\phi\rangle^c &= \left(\prod_i\left(\frac{\partial}{\partial\lambda_i}\right)^{n_i}\right) \\
&\quad\times\ln\langle\phi|e^{\alpha S^+}\prod_i e^{\lambda_i A_i}e^{\beta S}|\phi\rangle|_{\lambda_i=0\forall i} \\
&= \langle e^{\alpha S}\phi|\prod_i A_i^{n_i}|e^{\beta S}\phi\rangle^c. \qquad \text{(A.4)}
\end{aligned}$$

In the last equation we have reintroduced (generalized) cumulants, now formed with the bra state $\langle e^{\alpha S}\phi|$ and the ket state $|e^{\beta S}\phi\rangle$. With $\alpha=\beta=1$ we obtain the desired result (A.1).

Explicitly we find from (A.1):

$$\begin{aligned}
\langle\phi|e^{S^+}A\,e^S\,|\phi\rangle^c &= \frac{\langle\phi|e^{S^+}A\,e^S|\phi\rangle}{\langle\phi|e^{S^+}e^S|\phi\rangle}, \\
\langle\phi|e^{S^+}AB\,e^S|\phi\rangle^c &= \frac{\langle\phi|e^{S^+}AB\,e^S|\phi\rangle}{\langle\phi|e^{S^+}e^S|\phi\rangle} \\
&\quad - \frac{\langle\phi|\,e^{S^+}A\,e^S|\phi\rangle\langle\phi|e^{S^+}B\,e^S|\phi\rangle}{\langle\phi|e^{S^+}e^S|\phi\rangle^2}, \qquad \text{(A.5)}
\end{aligned}$$

and so on.

References

1. J. Orenstein, *et al.*, Phys. Rev. B **42**, 6342 (1990); S. Uchida, *et al.*, Phys. Rev. B **43**, 7942 (1991).
2. E. Dagotto, Rev. Mod. Phys. **66**, 763 (1994).
3. T. Tohyama, P. Horsch, S. Maekawa, Phys. Rev. Lett. **74**, 980 (1995).
4. R. Eder, Y. Ohta, Phys. Rev. B **51**, 11683 (1995).
5. R. Eder, Y. Ohta, S. Maekawa, Phys. Rev. Lett. **74**, 5124 (1995).
6. R. Eder, P. Wrobel, Y. Ohta, Phys. Rev. B **54**, 11034 (1996).
7. J. Jaklic, P. Prelovsek, Phys. Rev. B **52**, 6903 (1995).
8. Z. Wang, Y. Bang, G. Kotliar, Phys. Rev. Lett. **67**, 2733 (1991); Y. Bang, G. Kotliar, Phys. Rev. B **48**, 9898 (1993).
9. L. Gehlhoff, R. Zeyher, Phys. Rev. B **52**, 4635 (1995).
10. D.K.K. Lee, D.H. Kim, P.A. Lee, Phys. Rev. Lett. **76**, 4801 (1996).
11. G. Khaliullin, P. Horsch, Phys. Rev. B **54**, 9600 (1996).
12. R. Zeyher, M.L. Kulic, Phys. Rev. B **54**, 8985 (1996).
13. P.W. Anderson, Science **235**, 1196 (1987).
14. F.C. Zhang, T.M. Rice, Phys. Rev. B **37**, 3759 (1988).
15. H. Mori, Progr. Theor. Phys. **34**, 423 (1965).
16. R. Zwanzig, *Lectures in Theoretical Physics* (New York, Interscience, 1961) Vol. 3.
17. D. Forster, *Hydrodynamic Fluctuations, Broken Symmetry, and Correlation Functions* (Reading, MA: Benjamin, 1975).
18. M. Vojta, K.W. Becker, Europhys. Lett. **38**, 607 (1997).
19. K.W. Becker, P. Fulde, Z. Phys. B **72**, 423 (1988).
20. K.W. Becker, H. Won, P. Fulde, Z. Phys. B **75**, 335, (1989).
21. K.W. Becker, W. Brenig, Z. Phys. B **79**, 195 (1990).
22. R. Kubo, J. Phys. Soc. Jpn **17**, 1700 (1962).
23. M. Vojta, K.W. Becker, Ann. Phys. (Leipzig) **5**, 156 (1996); M. Vojta, K.W. Becker, Phys. Rev. B **54**, 15483 (1996).
24. T. Schork, P. Fulde, J. Chem. Phys. **97**, 9195 (1992).
25. Y. Nagaoka, Phys. Rev. **147**, 392 (1966).
26. W.F. Brinkman, T.M. Rice, Phys. Rev. B **2**, 1324 (1970).
27. S.A. Trugman, Phys. Rev. B **37**, 1597 (1988).
28. B.I. Shraiman, E.D. Siggia, Phys. Rev. Lett. **60**, 740 (1988).
29. J.R. Schrieffer, X.G. Wen, S.C. Zhang, Phys. Rev. Lett **60**, 944 (1988).
30. K.W. Becker, R. Eder, H. Won, Phys. Rev. B **45**, 4864 (1992).
31. C.L. Kane, P.A. Lee, N. Read, Phys. Rev. B **39**, 6880 (1989).
32. K. Kladko, P. Fulde, Int. J. Quant. Chem. **66**, 377 (1998).